Role of MoO_3 /ZnO substitutions on radiation shielding and mechanical characteristics of lead silicate glasses

E. A. Abdel Wahab [a,*], Ateyyah. M. Al-Baradi [b], Kh. S. Shaaban [c]
[a] *Physics Department, Faculty of Science, Al-Azhar University, Assiut, P.O 71524, Egypt*
[b] *Department of Physics, College of Science, Taif University, P.O. Box 11099, Taif 21944, Saudi Arabia*
[c] *Department of Chemistry, Faculty of Science, Al-Azhar University, P.O. 71524, Assiut, Egypt*

In the composition range of x= 0-5 mol%, glasses in the system $60SiO_2$-$35Pb_3O_4$-$(5-x)$ ZnO-xMoO_3 have been investigated. An amorphous network structure characterizes the glasses. The density values for the LZSM glasses scaled between 5.91 g/cm³ for Mo0 and 6.249 g/cm³ for Mo5. The ultrasonic technique indicates that the shear and longitudinal speeds (V_T & V_L) increase linearly as the amount of MoO_3 substituted for ZnO in the fabricated glasses increases. The elastic moduli were calculated and found to be increased with an increase in both ultrasonic velocities and density of the glass, which suggests a correlation between these parameters in the fabricated glasses. The radiation attenuation capacity with the addition of MoO_3 increased systematically, which indicates the role of MoO_3 in modifying the glass composition and enhances its ability to attenuate against harmful radiation. Mo5 establishes excellent protective resources compared to other substances, so Mo5 develops a favorable selection for building radiation absorption blocks. Such blocks show an acute character in protecting both nature and a person's health versus the dangerous impacts of radiation exposure.

(Received August 16, 2024; Accepted October 16, 2024)

Keywords: MoO_3 glasses, Elastic moduli, HVL, MFP

1. Introduction

Silicate glasses have established the most global glass type, developing from the solidification of the amorphous of melted silicon dioxide (SiO_2). The pioneer characteristics like chemical durability and strong stable network structure formed by Si^{4+} cations tetrahedrally coordinated with oxygen anions (O^{2-}). This hardy network allows brilliant resistance to corrosion and weathering. Furthermore, the ability of the network to assist diverse modifying cations and the fundamental transparency of silica provide silicate glasses with excellent usefulness. These properties make them invaluable across diverse applications, including architectural windows and containers, optical lenses, optical fibers, and specialized glasses for scientific instruments demanding high chemical and thermal resistance. [1-4]. These glasses provide structural integrity, protection against UV radiation, and resistance to impact and breakage [5-8].

Zinc oxide (ZnO) and lead oxide (PbO) are strategically incorporated into silicate glasses due to their distinct effects on the glass network structure and material properties. ZnO functions as a network former, readily integrating into the silica network through strong covalent Si-O-Zn linkages. This enhances network connectivity, leading to improved chemical durability against weathering and corrosion. Additionally, ZnO has a high packing density that contributes to increased mechanical strength and fracture toughness, making the glass more resistant to deformation and crack propagation. [9-13]. The interplay between ZnO and PbO allows for the tailoring of glass properties. ZnO strengthens the network and enhances durability, while PbO modifies the refractive index and lowers the melting point. This combination makes these oxides valuable tools for creating glasses with a diverse range of functionalities for applications in optics, radiation shielding, and other specialized fields. [14-19].

* Corresponding author: essam.ah77@gmail.com
https://doi.org/10.15251/JOR.2024.205.731

Molybdenum trioxide (MoO_3) presents a compelling avenue for investigation in Pb_3O_4-ZnO-SiO_2 glass systems, particularly regarding their mechanical and radiation shielding properties [20-22]. Due to its high atomic number and density, akin to lead and zinc cations, MoO_3 holds promise for further enhancing these functionalities in the glass. Recent research efforts have been directed towards elucidating the structure-property relationships in MoO_3-doped Pb_3O_4-ZnO-SiO_2 glasses. These studies aim to systematically delineate how varying MoO_3 concentrations influence the glass's radiation shielding efficacy, mechanical robustness, and optical characteristics. [23-25]. The potential impact of substituting ZnO with MoO_3 in Pb_3O_4-ZnO-SiO_2 glasses presents a captivating way for scientific exploration. This study delves into this strategic substitution, aiming to clarify its influence on both the mechanical properties and gamma-ray attenuation capabilities of the resulting glass system. Through particular investigation, we aspire to contribute novel and significant insights to the existing frame of knowledge regarding the mechanical and radiation shielding behaviors of glasses. This study delves into the potential of molybdenum oxide (MoO_3) as a substitute for zinc oxide (ZnO) in Pb_3O_4-ZnO-SiO_2 glasses. We aim to systematically evaluate the influence of this compositional modification on a comprehensive array of material properties, encompassing physical, mechanical, and radiation shielding characteristics to use this glass as a shield from X and gamma rays.

Samples code:

Mo0 version sample.
Mo1 sample with 1 mol.% MoO_3.
Mo2 sample with 2 mol.% MoO_3.
Mo4 sample with 4 mol.% MoO_3.
Mo5 sample with 5 mol.% MoO_3.

2. Glasses preparation

2.1. Fabrication of samples

Table 1 summarizes the glasses based on the chemical composition Pb_3O_4-ZnO-SiO_2, with MoO_3 doping. The combinations are heated by an electric furnace and the technique of melt-quenching takes place at 1200 °C. Immediately, the mix is completely melted and homogenized, it is streamed on a heated stainless-steel molding. After pouring the liquid glass onto the mold, it is directly transported to an alternative oven that is set at 400 °C. There were two kinds of glass samples: granules and bulk.

Table 1. The compositions in mol. and W.%.

Code					Compositions				
	SiO_2	Pb_3O_5	ZnO	MoO_3	Si	Pb	Zn	Mo	O
Mo0	**60**	**35**	**5**	**0**	0.2805	0.3173	0.0402	0.0000	0.3620
Mo1	**60**	**35**	**4**	**1**	0.2805	0.3173	0.0321	0.0067	0.3634
Mo2	**60**	**35**	**2**	**3**	0.2805	0.3173	0.0241	0.0133	0.3648
Mo4	**60**	**35**	**1**	**4**	0.2805	0.3173	0.0080	0.0267	0.3675
Mo5	**60**	**35**	**0**	**5**	0.2805	0.3173	0.0000	0.0333	0.3689

2.2. Tools

Xylene liquid was used as an immersed solution to calculate the glass density by the following formula: $\rho = (\frac{Wa}{Wa-Wb})0.86$ (g/cm³), which is known as Archimedes' suggestion, hence W_a termed the sample weight in air and W_b identified the immersed weight.

The pulse-echo method is a valuable technique for measuring the transverse (V_T) and longitudinal (V_L) velocities of the specimens. The KARL DEUTSCH Echograph model 1085 is a specific instrument designed for ultrasonic testing and non-destructive evaluation, making it well-suited for this purpose. The exact mechanical factor evaluation formulae are referenced in [26-30].

The X'Pert Pro Panalytical diffractometer was used to measure and analyze the XRD pattern of the present samples.

EPiXS software was used to utilize the radiation shielding parameters [31], it is friendly user software given the factors MAC, LAC, MFP, HVL, BEF, BAEF $Z_{eff,}$ and N_{eff}.

3. Results and discussion

3.1. XRD analysis

Fig. 1 describes the diffraction patterns (XRD) obtained from Mo^{3+} co-doped ZnO-SiO_2-Pb_3O_4 samples within the angular range of $10° \leq 2\theta \leq 90°$. Notably, the observed pattern deviates significantly from the sharp peaks characteristic of crystalline materials. Instead, a broad hump is evident, indicative of the fleeting variety or confined structural collections contained by the amorphous glass network. This broad hump signifies the absence of long-range order in the material, a describing feature of formless solids (glasses). While long-range order implies a repeating periodic arrangement of atoms throughout the entire material, present fabricated samples lack this repetitive structure. [32-35].

3.2. Physical parameters

Table **2** offers the details about the calculated density (ρ) and molar volume (V_m) for the fabricated specimens. A clear trend emerges MoO_3 incorporation leads to a systematic increase in density compared to the undoped base glass (Mo0). This observation can be attributed to the contrasting molecular masses of Molybdenum (143.938 g/mol) and Zinc oxide (81.389 g/mol). As MoO_3 replaces ZnO, a heavier element is introduced into the glass network. This effectively increases the mass packing fraction within the same volume compared to the ZnO-containing counterpart. Consequently, MoO_3 appears to occupy more vacant spaces within the glass matrix, leading to a densification effect and a corresponding decrease in molar volume [36-41].

Table 2. Structural and physical characteristics of LZS glasses doped Mo ions.

Samples	Mo0	Mo1	Mo2	Mo4	Mo5
ρ, Density g/cm^3	5.91	5.96	6.04	6.174	6.249
V_m , Molar volume cm^3	47.39	47.10	46.58	45.77	45.32
OPD, packing density of oxygen	55.92	56.69	57.75	59.65	60.68
V_o, Molar volume of oxygen	17.88	17.64	17.31	16.76	16.48
ΔX, Electronegativity	1.402	1.3969	1.3918	1.3816	1.3765
F, Field strength (10^{16})	0	1.432	2.290	3.678	4.296

The molar volume of oxygen V_o and OPD for the MoO_3-doped lead zinc silicate glasses were determined and explored in Table **2**. A noteworthy observation is the concurrent increase in OPD and decreases in V_o with increasing MoO_3 content. This compelling evidence suggests that MoO_3 doping leads to a more condensed composition of O^{-2} atoms inside the glass network. The observed inverse correlation between OPD and V_o reinforces this investigation. A higher OPD signifies a denser packing of oxygen particles inside a specific volume, while a lower V_o indicates a reduction in the average space captured by each oxygen atom. The good agreement between these two parameters underscores a uniform tendency in the structural modifications produced by MoO_3 incorporation. [42-44].

The electronegativity (Δx) of the present specimens was estimated using the electronegativity difference between the glass individual components ($for\ Si-O\ =\ 1.54, Pb-O\ =\ 1.11, Zn-O = 1.79\ and\ Mo-O\ =1.64$) Pauling scale. The following equation has been utilized to investigate its values.

$$\Delta x = \sum_i N_i \Delta x_i \ , \quad \Delta x_i = x_{An} - x_{Ca} \tag{1}$$

N_i denotes the ratio of oxides and Δx_i refer to the Electronegativity difference between the cation and an anion in every composition in the present samples. The present result values are explored in Table **2**. The data indicate that Δx decreases with increased molybdenum content in the present glass sample. Fig. **2** shows the relationship between field strength (F), interionic distance, and polaron radius against the concentration of MoO_3 it is clear from the result that F increases with supplementary of Mo ion in the fabricated glasses while both R_i and R_p decrease.

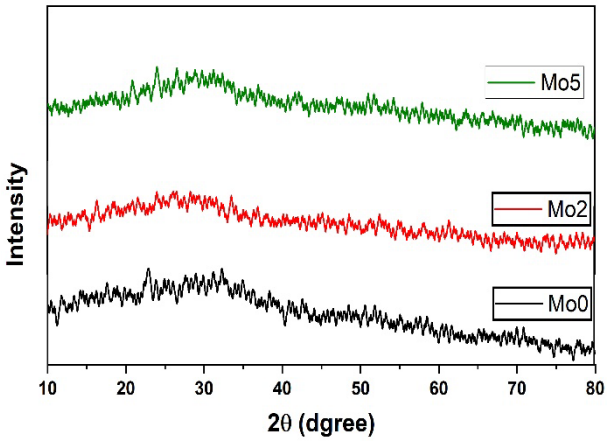

Fig. 1. XRD pattern of the present glass samples.

3.3. Mechanical characteristics

The observations of V_L&V_T are revealed in Fig. **3** and Table **3**. Fig. **3** depicts a trend where both (V_L&V_T), increase linearly as the amount of MoO_3 substituted for ZnO in the fabricated glasses increases. The (V_L&V_T), increases from 4790 to 5185 m/s and 2385 to 2780 m/s as the content of MoO_3 grows from 0 to 5 mol%. The explanation implies that the addition of MoO_3 to the SiO_2–Pb_3O_4–ZnO glass specimens results in an alteration of the internal glass network, leading to the creation of interstitial gaps or unoccupied spaces within the structure. This alteration subsequently contributes to the observed increases in ultrasonic velocities [45-51].

Fig. 4 and Table **3** illustrate the estimation of elastic moduli using the observed ultrasonic velocities. The observed increase in elastic moduli, along with increases in ultrasonic velocities and density of the glass, suggests a correlation between these parameters in the fabricated glasses. An increase in elastic moduli indicates that the glass becomes stiffer or more resistant to deformation. The incorporation of MoO_3 increases the overall density of the glass due to its higher atomic mass compared to ZnO.

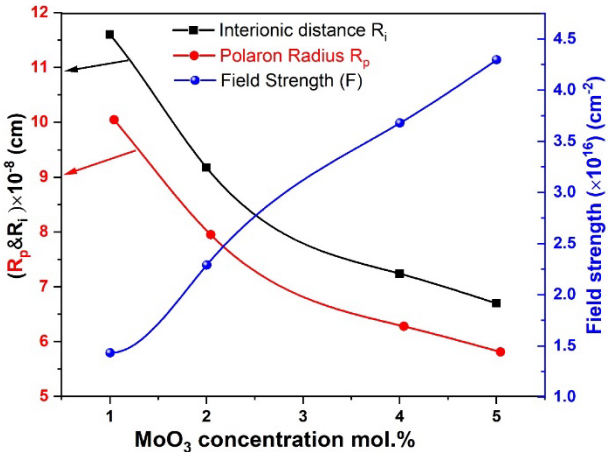

Fig. 2. R_i, R_p, and F of the present glass as a function of MoO_3 content.

The higher density contributes to the increased stiffness and ultrasonic velocities observed in the fabricated glasses. The increases in elastic moduli of the glasses were attributed to rises in cross-link densities and the number of bonds in the glass samples. The correlation between elastic moduli and ultrasonic wave velocities indicates a strong relationship between the glass's bond types and its mechanical properties. Ultrasonic wave velocities are influenced by the stiffness and density of a material, which in turn are influenced by the types of bonds present. Glasses with stronger bonds tend to have higher velocities because the waves propagate more efficiently through a stiffer medium. By correlating the elastic moduli (which reflect the glass's stiffness) with ultrasonic wave velocities, researchers can infer information about the types and strengths of bonds present in the glass. For instance, if an increase in elastic moduli is accompanied by an increase in wave velocities, it suggests that the material has become stiffer due to changes in its bonding structure. Overall, the correlation between elastic moduli and ultrasonic wave velocities serves as a powerful tool for studying the relationship between bond types and mechanical properties in glasses [45-51]. The addition of MoO_3 to SiO_2-based glasses has been reported to enhance their mechanical properties in various studies [10, 43, and 49]. When incorporated into SiO_2-based glasses, MoO_3 can alter the network connectivity and introduce favorable interactions that lead to improved mechanical strength, hardness, and other mechanical properties. Overall, the addition of MoO_3 to glass compositions offers a promising approach to enhancing their mechanical properties, including microhardness (H). The significant increase in microhardness from 3.69 to 6.49 GPa underscores the effectiveness of MoO_3 addition in enhancing the mechanical properties of the glass. This improvement is valuable for various applications where hardness and and high-performance optical components.

The Makishima-Mackenzie model (MMM) [52-53] is a widely used approach in materials science for predicting the elastic properties of glasses based on their composition. It is particularly useful for studying the effects of dopants or additives on these properties. Fig. **5** and Table **3** illustrate scratch resistance are critical, such as in the production of durable coatings, protective layers, the estimation of elastic moduli using this model. The discovered values for Young's modulus (Y_{th}), between 46.41-51.65 GPa, and longitudinal modulus (L_{th}), between 50.58-57. 5 GPa, shear modulus (G_{th}) between 21.91-23.73 GPa, and bulk modulus (K_{th}) between 21.37-25.86 GPa exhibited by the MoO_3-doped silicate glasses under investigation. The observed increase in elastic modulus when ZnO is substituted with MoO_3 in the glass network is due to the increase in the coordination number of Mo than Zn. The packing density (V_i) and dissociation energy (G_i) of glasses are two of the variables that might affect their elastic modulus. As the MoO3 increased the (V_i) increased from 0.385 to 0.419 and (G_i) increased from 14.419 to 14.757. Fig. **6** presents a graphical representation of the relationship between (G_i) & (V_i) for the investigated glasses.

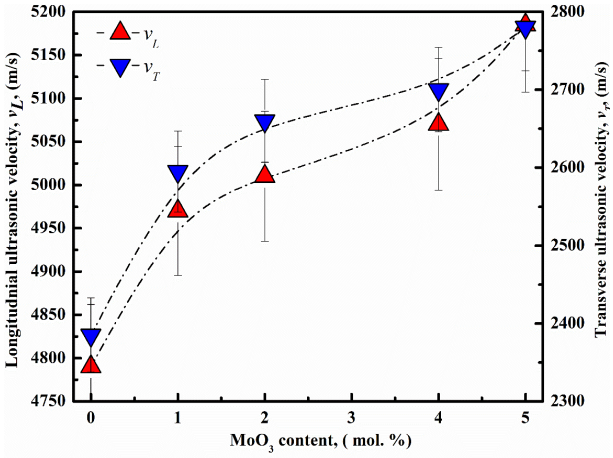

Fig. 3. Longitudinal and shear ultrasonic velocities (V_L&V_T), of $60SiO_2$-$35Pb_3O_4$ – $(5-x)$ ZnO-$xMoO_3$ glasses.

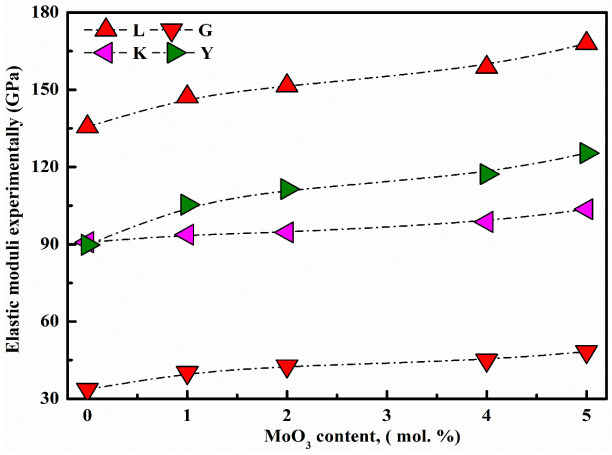

Fig. 4. Experimental elastic moduli of $60SiO_2$-$35Pb_3O_4$ – $(5-x)$ ZnO-$xMoO_3$ glasses.

Overall, the application of high-strength glass in various aspects of our lives enhances safety, durability, and performance across different industries and sectors. Strengthened glass materials play a crucial role in protecting individuals, property, and infrastructure, while also contributing to technological advancements and innovation. High-strength glass finds applications in specialized industries and sectors, including aerospace, defense, marine, and sports equipment. It is used for manufacturing aircraft windows, submarine portholes, bulletproof glass, and sporting goods, such as helmets and protective eyewear. Strengthened glass materials provide critical protection against extreme conditions, impacts, and hazards, ensuring the safety and performance of equipment and personnel. In the medical industry, high-strength glass is utilized for manufacturing medical devices and equipment, such as laboratory glassware, diagnostic instruments, and surgical tools. In the automotive industry, high-strength glass is used for manufacturing windshields and windows to improve passenger safety and vehicle durability. High-strength glass is essential for safety glazing applications in buildings and structures.

Table 3. Mechanical aspects data of LZS glasses doped with MoO_3.

parameters	**Mo0**	**Mo1**	**Mo2**	**Mo4**	**Mo5**
V_L (m/s)	4790	4970	5010	5070	5185
V_S (m/s)	2385	2595	2660	2700	2780
L (GPa)	135.6	147.24	151.6	158.7	168
G (GPa)	33.6	40.1	42.7	45	48.3
K (GPa)	90.8	93.7	94.6	98.7	103.6
Y (GPa)	89.77	105.38	111.4	117.2	125.4
H(GPa)	3.7	5.0	5.6	5.9	6.5
V_i(cm^3/mol)	0.39	0.39	0.40	0.41	0.42
G_i(KJ/cm^3)	14.42	14.49	14.55	14.69	14.76
L_{th}*(GPa)*	50.58	51.72	53.18	55.98	57.5
G_{th}*(GPa)*	21.91	22.22	22.60	23.34	23.73
K_{th}*(GPa)*	21.37	22.10	23.04	24.86	25.86
Y_{th}*(GPa)*	46.41	47.30	48.41	50.52	51.65

3.4. Radiation shielding studies

The linear attenuation coefficient (μ) quantifies how effectively a material weakens the beam as it travels through. A higher μ signifies a stronger interaction, leading to a more rapid decrease in the intensity of the transmitted radiation. This coefficient essentially describes the probability of a single photon (X-ray or gamma ray) being absorbed or scattered per unit distance traveled within the material. By measuring the original and transmitted radiation intensities, and knowing the material depth, the linear coefficient attenuation can be utilized to calculate various aspects of radiation interaction, making it a crucial parameter in diverse fields like medical imaging, radiation shielding design, and material characterization.

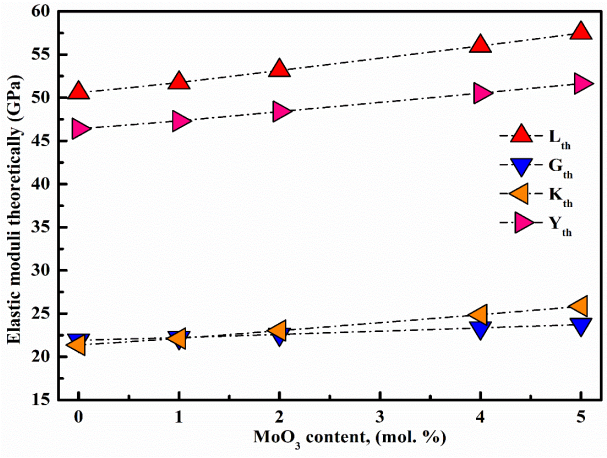

Fig. 5. Theoretically elastic moduli of $60SiO_2$-$35Pb_3O_4$ – $(5-x)$ ZnO-$xMoO_3$ glasses.

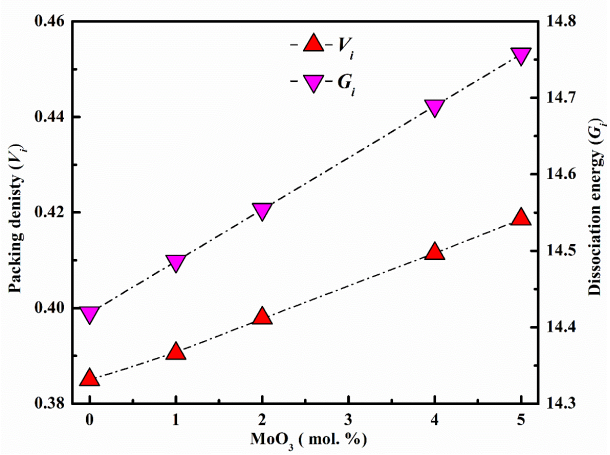

Fig. 6. The packing density (V_i) and dissociation energy (G_i) of $60SiO_2$-$35Pb_3O_4$ – $(5-x)$ ZnO-$xMoO_3$ glasses.

The linear attenuation coefficient (LAC) for $(5-x)$ZnO-$x$$MoO_3$-$60SiO_2$-$35Pb_3O_4$ glasses has been evaluated as [54-56]:

$$\mu = \frac{Ln(\frac{I_o}{I})}{d} \tag{2}$$

Figs. **7** represents the (μ) for lead-zinc-silicate glass-doped molybdenum. The (μ) cm^{-1} values For Mo0 range from 0.193to 248.8, for Mo1 ranges from 0.194 to 248.18, for Mo2 ranges from 0.197 to 248.73, for Mo4 ranges between 0.202 and 248.55, and Mo5 ranges between 0.204 and 248.69. The (μ) shows significant variations with energy overall, for a range of energies from 15 keV to 100 keV, one can deduce that μ is a great value and rapidly decline. The persistence of (μ) outside the 100 keV edges, although at a relaxed speed as the energy of photons rises more. This behavior can be explained as, at the small energy at the end of the radiation spectrum, photoelectric absorption (PE) reigns dominant as the primary contributor to high attenuation coefficients. The attenuation coefficient (μ) rapidly decreases as photon energy (E) increases, which is an important finding. Another process that can occur, the Compton scattering (CS) probability, becomes more noticeable when E increases outside the PE dominance zone. The confined electrons cause the photons to lose some of their energy throughout this process. The attenuation coefficient decreases more slowly at higher energy as a result of this change in dominance from PE to CS[54-58].

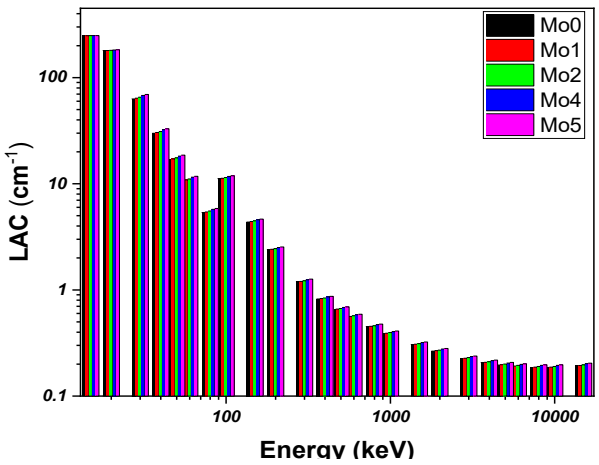

Fig. 7. LAC for the present samples at various MoO_3 content.

This study shows a clear correlation between MoO_3 content and the photon attenuation of glasses capacity, as evidenced by the increasing trend in the linear attenuation coefficient (μ). Molybdenum asserts a significantly extreme atomic quantity compared to zinc (Zn). This higher Z translates to a greater interaction with photons, particularly through mechanisms like the photoelectric effect. As the MoO_3 content increases from Mo0 to Mo5, a corresponding improvement in the linear attenuation coefficient is observed. This compelling evidence suggests that MoO_3 incorporation effectively enhances the ability of the specimens to weaken incident radiation [55-57].

Designing and optimizing radiation shielding solutions for a variety of applications requires an understanding of the half-value layer (HVL) concept. HVL is vital for maintaining safety and reducing radiation exposure, from the complex shielding needs of medical imaging equipment to the strong barriers used in nuclear power plants. The HVL of present samples has been estimated from the following connections,

$$HVL = \frac{0.693}{MAC} \tag{3}$$

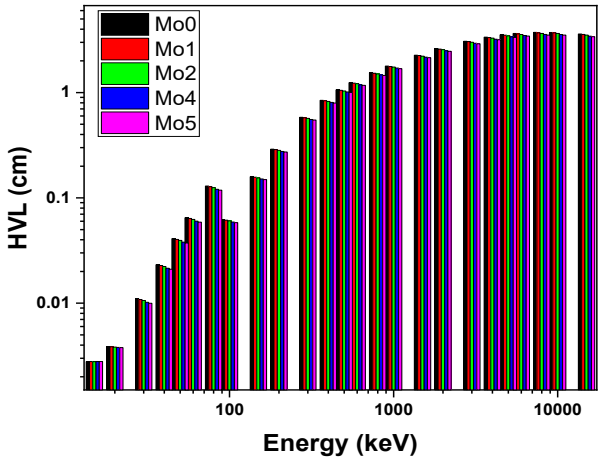

Fig. 8. HVL for the present samples at various MoO_3 content.

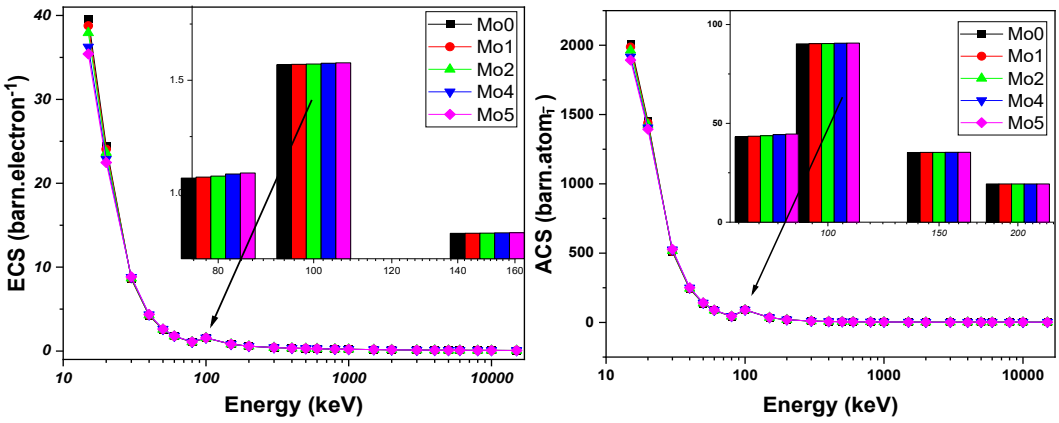

Fig. 10. ACS for the present samples at various MoO_3 content.

Fig. **8** shows the correlation linking (E) and the matching HVL quantities for lead zinc silicate glasses. In the lower range of 15-500 keV, the HVL values for Mo0 and Mo5 specimens are as follows (0.002786–1.060) cm, and (0.00279– 1.0012) cm. It shows that as the phenomena E improves to 5000 keV, the quantity of HVL representing Mo0 and Mo5 specimens also enhances.

For Mo0 the HVL was 3.54 cm and for Mo5 the HVL was 3.34 cm. These values of HVL characterize the length inside the specimens of glass needed to decrease the beam of incoming radiation to fifty percent at 5000 keV photon energy. Remarkably Mo5 specimen demonstrates smaller half-value layer values compared to the Mo0 specimen. This implies that the Mo5 sample is further relevant to weakening radiation, needing less depth to get the identical intensity of radiation decline.

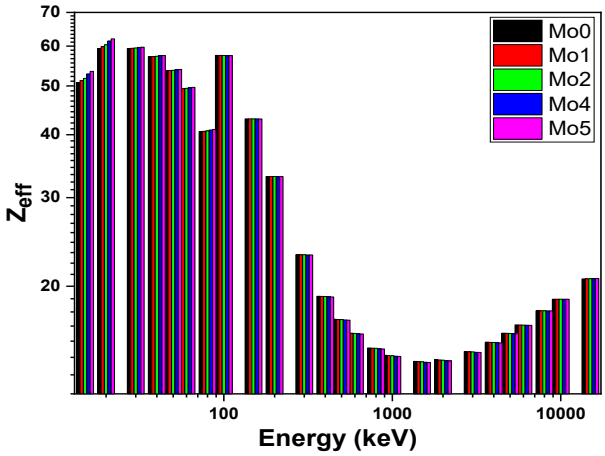

Fig. 11. Z_{eff} for the present samples at various MoO_3 content.

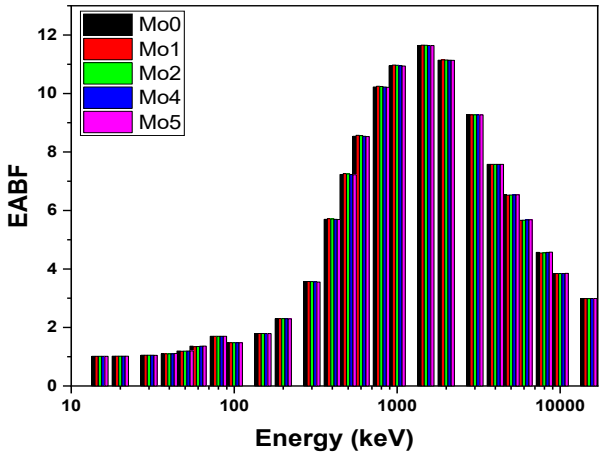

Fig. 12. EABF for the present samples at various MoO_3 content.

The addition of MoO_3 systematically increases the radiation attenuation capacity, indicating that changing the glass composition improves the specimens' competence to shield alongside ionizing radiation. This discovery shows that it is possible to modify the network of glasses such as LZSM to enhance the competence of radiation attenuation capabilities, which is important for radiation shielding applications.

The cross-section σ_m of molecular content of the present glasses can be determined as the following estimation[16, 54- 58]

$$\sigma_m = (\frac{\mu}{\rho})(\frac{M}{N_A}) \quad (2)$$

The cross-section σ_a of the whole-entire atoms included in the present specimens can also be estimated from the equation:

$$\sigma_a = \sigma_m \ / \sum I \ n_i \quad (3)$$

when n_i is the formula unit number.

At the end of these parameters, the effective number (Z_{eff}) of the whole atoms included in the glasses can be established by the arising connection [54, 55]

$$Z_{eff} = \frac{\sigma_a}{\sigma_e} \quad (4)$$

where σ_e is the sum cross-section of the electron.

Fig. **9** and **10** explore graphs showing the relationships between (ECS)& (ACS) and the incident gamma photon energy for the present glasses. As the figures the Mo5 glass regularly exhibits a maximum (ECS and ACS) at all energies associated with other specimens, which implies that Mo5 glass is more valuable in attenuating radiation. A Higher (ECS and ACS) signifies that photons extra interact with the Mo5 specimen across smaller gaps, efficiently decreasing its entrance among the substance. Consequently, the Mo5 specimen is more competent at attenuating radiation [55-58].

The effective atomic number Z_{eff} has been considered in the present work as shown in Fig. **11.** It was found that by supplying MoO_3 in the present glass the Z_{eff} increases. This behavior is because the atomic number of molybdenum is higher than the atomic number of zinc. In Fig. **12** and **13** the buildup exposure factor (BEF) and energy absorption build factor (EABF) were explored. As the figures the concentration of Mo ions modifies the glass network to be an effective material against the gamma-ray [54-58]. Finally, the R factor takes place in the present study and it increases with an increase in the photon energy and has a maximum energy of 1500 keV and it declines again after that value. Also, it is affected by the concentration of molybdenum ions content in present glass specimens as shown in Fig. **14**. As a result, sample Mo5 shows better-shielding properties than other materials, making it a viable option for creating radiation absorption shields. These barriers are essential for protecting the environment and public health from the damaging effects of radiation exposure.

4. Conclusions

Mo^{3+} co-doped $60SiO_2$-$35Pb_3O_4$ - 5ZnO samples with the composition $60SiO_2$-$35Pb_3O_4$-$(5-x)$ ZnO-xMoO_3, x=0, 1, 2, 4, and 5 mol% have been successfully fabricated with melt-quench method. Confirmation of the amorphous nature of LZSM glass has been using XRD. The density values for the LZSM glasses range from 5.91 g/cm³ for $LZSM_0$ to 6.249 g/cm³ for $LZSM_5$. The longitudinal and shear ultrasonic velocities (V_L&V_T) increase linearly as the amount of MoO_3 substituted for ZnO in the fabricated glasses increases. The (V_L&V_T), increases from 4790 to 5185 m/s and 2385 to 2780 m/s as the concentration of MoO_3 increases from 0 to 5 mol%. The observed increase in elastic moduli, along with increases in ultrasonic velocities and density of the glass, suggests a correlation between these parameters in the fabricated glasses. An increase in elastic moduli indicates that the glass becomes stiffer or more resistant to deformation. The findings show that the LAC values follow the following trend. In cm^{-1}, Mo0<Mo1<Mo2<Mo4<Mo5. The introduction of MoO_3 systematically increases the radiation attenuation capacity, indicating that changing the composition of the glass improves the ability of specimens to shield against gamma radiation. Because Mo_5 exhibits better shielding qualities than other materials, it becomes a possible option for creating a radiation absorption shield. These shields are essential for protecting nature and community health from the damaging effects of radiation exposure.

Acknowledgments

The authors extend their appreciation to Taif University, Saudi Arabia, for supporting this work through project number (TU-DSPP-2024-124).

References

[1] Alzahrani, A. S., Aloraini, D. A., Wahab, E. A. A., et al. Silicon **16**, 2401–2413 (2024); https://doi.org/10.1007/s12633-024-02846-8
[2] Aloraini, D. A., Ashour, A., & Shaaban, K. S., Silicon, 16 1837–1846(2023); https://doi.org/10.1007/s12633-023-02804-w
[3] Shaaban, K. S., Al-Baradi, A. M., & Ali, A. M., Silicon **14**(11), 8971–8979(2022); https://doi.org/10.1007/s12633-022-01702-x
[4] Wahab, E. A. A., Alyousef, H. A., El-Rehim, A. F. A., et al., Journal of Electronic Materials, **52**(1), 219–236(2023); https://doi.org/10.1007/s11664-022-09969-x
[5] Shaaban, K. S., Alomairy, S., & Al-Buriahi, M. S., Journal of Materials Science: Materials in Electronics, **32**(22), 26034–26048(2021). https://doi.org/10.1007/s10854-021-05885-8
[6] Rammah, Y. S., El-Agawany, F. I., Wahab, E. A. A., Hessien, M. M., & Shaaban, K. S., Radiation Physics and Chemistry, **193**, 109956(2022); https://doi:10.1016/j.radphyschem.2021.109956
[7] El-Rehim, A. F. A., & Shaaban, K. S., Journal of Materials Science: Materials in Electronics, **32**(4), 4651–4671(2021); https://doi:10.1007/s10854-020-05204-7
[8] Basha, B., Shaaban, K. S., & Abdel Wahab, E. A., . Digest Journal of Nanomaterials and Biostructures, **18**(2), 713–726 (2023); https://doi.org/10.15251/DJNB.2023.182.713
[9] Shaaban, K. S., Al-Baradi, A. M., & Ali, A. M., Journal of Materials Science: Materials in Electronics, **33**(12), 3297–3305(2022); https://doi.org/10.1007/s10854-021-07530-w
[10] Alomairy, S., Alrowaili, Z. A., Kebaili, I., et al., Silicon, **14**(12), 5661–5671(2022) ; https://doi.org/10.1007/s12633-021-01347-2
[11] Shaaban, K.S., Saddeek, Y.B., Silicon **9**, 785–793(2017) ; https://doi.org/10.1007/s12633-017-9558-5
[12] Shaaban, K. S., Alotaibi, B. M., Alharbiy, N., et al., Applied Physics A, **128**(3), 333(2022); https://doi.org/10.1007/s00339-022-05474-4
[13] Shaaban, K. S., Boukhris, I., Kebaili, I., et al., Silicon, **14**(8), 3091–3100(2022); https://doi.org/10.1007/s12633-021-01080-w
[14] Althagafi, T. M., Sayed, M. A., Alghasham, H. A., et al., Silicon, **15** 7047–7056(2023); https://doi.org/10.1007/s12633-023-02567-4
[15] Shaaban, K.S., Abo-Naf, S.M., & Hassouna, M.E.M., Silicon, **11**, 2421–2428(2019); https://doi.org/10.1007/s12633-016-9519-4
[16] Shaaban, K.S., Abo-naf, S.M., Abd Elnaeim, A.M., et al., Applied Physics A, **123**, 457(2017); https://doi.org/10.1007/s00339-017-1052-9
[17] Shaaban, K. S., Althagafi, T. M., Ashour, A., Alalawi, A., Al-Buriahi, M., & Ibraheem, A. A., Radiation Physics and Chemistry, **216**, 111440(2024); https://doi.org/10.1016/j.radphyschem.2023.111440
[18] Almutairi, H.M., Aloraini, D.A., Alsafi, K. et al., Silicon, **16** 2873–2884(2024) ; https://doi.org/10.1007/s12633-024-02900-5
[19] Aloraini, D. A., Almutairi, H. M., Alzahrani, A. S., et al., Silicon, **16**, 2791–2800(2024). https://doi.org/10.1007/s12633-024-02855-7
[20] El-Maaref, A. A., Alotaibi, B. M., Alharbi, N., & et al., Journal of Inorganic and Organometallic Polymers and Materials, **32**,. 3117–3127(2022); https://doi.org/10.1007/s10904-022-02345-6
[21] Sayed, M.A., Basha, B., Al-Harbi, N. et al., Silicon **15**, 6463–6471(2023); https://doi.org/10.1007/s12633-023-02537-w

[22] Shaaban, K. S., Alotaibi, B. M., Algarni, S. A., & et al., Silicon, **14**(12), 10817–10826(2022); https://doi.org/10.1007/s12633-022-01784-7
[23] Hila, F.C., Asuncion-Astronomo, A., Dingle, C.A.M., Jecong, J.F.M., Javier-Hila, A.M.V., Gili, M.B.Z., Balderas, C.V., Lopez, G.E.P., Guillermo, N.R.D., Amorsolo, A.V., Jr, Radiation Physics and Chemistry, 109331(2021).
[24] Algarni, S. A., El-Maaref, A. A., Alotaibi, B. M., et al., Journal of Inorganic and Organometallic Polymers, **32**(2), 2873–2881(2022); https://doi.org/10.1007/s10904-022-02321-0
[25] Shaaban, K. S., Al-Baradi, A. M., & Ali, A. M., RSC Advances, **12**(5), 3036–3043(2022). https://doi.org/10.1039/d2ra00171c
[26] Sayyed, M. I., Sadeq, M. S., Shaaban, Kh. S., Abd El-Rehim, A. F., Ali, A. M., & Morshidy, H. Y., Optical Materials, **142**, 114051(2023); https://doi.org/10.1016/j.optmat.2023.114051
[27] Shaaban, K. S., Al-Baradi, A. M., & Wahab, E. A. A., Silicon, **14**(11), 5057–5065(2022); https://doi.org/10.1007/s12633-021-01309-8
[28] Ali, A. M., Alrowaili, Z. A., Al-Baradi, A. M., et al., Silicon, **14**(11), 6447–6455(2022); https://doi.org/10.1007/s12633-021-01440-6
[29] Alomairy, S., Aboraia, A. M., Shaaban, E. R., & Shaaban, K. S., Brazilian Journal of Physics, **51**(4), 1237-1248(2021); https://doi:10.1007/s13538-021-00928-1
[30] Sayyed, M. I., Morshidy, H. Y., Shaaban, K. S., Abd El-Rehim, A. F., Ali, A. M., & Sadeq, M. S., Optical Materials, **144**, 114300(2023); https://doi.org/10.1016/j.optmat.2023.114300
[31] Wahab, E. A. A., Ahmed, E. M., Rammah, Y. S., et al., Journal of Inorganic and Organometallic Polymers and Materials, **32**(7), 3983-3996(2022); https://doi.org/10.1007/s10904-022-02400-2
[32] Alrowaili, Z. A., Ali, A. M., Al-Baradi, A. M., et al., Optics and Quantum Electronics, **54**(4), 88(2022); https://doi.org/10.1007/s11082-021-03447-0
[33] Shaaban, K. S., Alotaibi, B. M., Alharbi, N., Alrowaili, Z. A., Al-Buriahi, M. S., Makhlouf, S. A., & Abd El-Rehim, A. F., Radiation Physics and Chemistry, **193**, 109995(2022); https://doi.org/10.1016/j.radphyschem.2022.109995
[34] Mahmoud, K., Alsubaie, A., Wahab, E.A.A., et al., Silicon, **14**(2), 3419-3427(2022); https://doi.org/10.1007/s12633-021-01125-0
[35] Shaaban, K. S., Alotaibi, B. M., Alrowaili, Z. A., Al-Buriahi, M. S., Ashour, A., & Yousef, S., Silicon, **15**(12), 5233-5243(2023); https://doi.org/10.1007/s12633-023-02433-3
[36] Shaaban, K. S., Al-Baradi, A. M., Alotaibi, B. M., & Abd El-Rehim, A. F., Journal of Materials Research and Technology, **23**, 756-764(2023); https://doi.org/10.1016/j.jmrt.2023.01.062
[37] Shaaban, K. S., Alrowaili, Z. A., Al-Baradi, A. M., et al., Silicon, **14**(11), 6457–6465(2022); https://doi.org/10.1007/s12633-021-01441-5
[38] Al-Baradi, A. M., Alotaibi, B. M., Alharbi, N., et al., Silicon, **14**(17), 10391–10399 (2022); https://doi.org/10.1007/s12633-022-01801-9
[39] Rammah, Y. S., El-Agawany, F. I., Wahab, E. A. A., Hessien, M. M., & Shaaban, K. S., Radiation Physics and Chemistry, **193**, 109956 (2022); https://doi.org/10.1016/j.radphyschem.2021.109956
[40] Almuqrin, A. H., Mahmoud, K. A., Wahab, E. A. A., Koubisy, M. S. I., Sayyed, M. I., & Shaaban, K. S., The European Physical Journal Plus, **136**(6), 133(2021); https://doi.org/10.1140/epjp/s13360-021-01564-z
[41] Alothman, M. A., Alrowaili, Z. A., Alzahrani, J. S., Wahab, E. A. A., Olarinoye, I. O., Sriwunkum, C., Shaaban, K. S., & Al-Buriahi, M. S., Journal of Alloys and Compounds, 882, (2021) 160625; https://doi.org/10.1016/j.jallcom.2021.160625
[42] Shaaban, K. S., Basha, B., Alrowaili, Z. A., Al-Buriahi, M. S., & Abdel Wahab, E. A., Radiochimica Acta, **111**(9), 713-724(2023); https://doi.org/10.1515/ract-2023-0140
[43] Varshneya, A. K., Gulf Professional Publishing, p. 33(1994).
[44] Makishima, A., & Mackenzie, J. D., Journal of Non-Crystalline Solids, **17** (2), 147-157(1975); https://doi.org/10.1016/0022-3093(75)90047-2
[45] Makishima, A., & Mackenzie, J. D., Journal of Non-Crystalline Solids, **12**(1), 35-45(1973); https://doi.org/10.1016/0022-3093(73)90053-7

[46] Wahab, E.A.A., Al-Baradi, A.M., Sayed, M.A., et al., Silicon, **14**, 8581–8597(2022); https://doi.org/10.1007/s12633-021-01652-w
[47] Kaky, K. M., Şakar, E., Akbaba, U., Emre Kasapoğlu, A., Sayyed, M., Gür, E., Baki, S., & Mahdi, M., Results in Physics, **14**, 102438(2019); https://doi.org/10.1016/j.rinp.2019.102438
[48] Tekin, H.O., ALMisned, G., Zakaly, H.M.H., Zamil, A., Khoucheich, D., Bilal, G., Al-Sammarraie, L., Issa, S.A.M., Al-Buriahi, M.S., Ene, A., Open Chem, 20, (2022) 130–145; https://doi.org/10.1515/CHEM-2022-0128
[49] Alghasham, H. A., Ismail, Y. A., Aloraini, D. A., & Shaaban, K., Materials Today Communications, **38**, 107840(2024); https://doi.org/10.1016/j.mtcomm.2023.107840
[50] Al-Buriahi, M. S., et al., **96**, 125325(2021); https://doi.org/10.1088/1402-4896/ac4121
[51] El-Rehim, A. F. A., Zahran, H. Y., Yahia, I. S., Wahab, E. A. A., & Shaaban, K. S., Journal of Materials Engineering and Performance, **30**(5), 1872–1884(2021); https://doi.org/10.1007/s11665-021-05513-w
[52] Laifi, J., Althagafi, T. M., Ibrahim, E. H., et al., Silicon, **15**(12), 5301-5314(2023) ; https://doi.org/10.1007/s12633-023-02699-7
[53] Alrowaili, Z. A., Al-Baradi, A. M., Sayed, M. A., Mossad Ali, A., Abdel Wahab, E. A., Al-Buriahi, M. S., & Shaaban, K. S., Optik, 168259(2021); https://doi.org/10.1016/j.ijleo.2021.168259
[54] Shaaban, K. S., Aloraini, D. A., Alsafi, K., Almutairi, H. M., Al Saleh, W. M., & Alzahrani, A. S., Materials Today communications, 38, 108309; https://doi.org/10.1016/j.mtcomm.2024.108309
[55] Shaaban, K. S., Alotaibi, B. M., Alharbiy, N., et al., Silicon, **14**(7), 11991-12000 (2022) ; https://doi.org/10.1007/s12633-022-02029-3
[56] Koubisy, M. S. I., Shaaban, K. S., Wahab, E. A. A., Sayyed, M. I., & Mahmoud, K. A., The European Physical Journal Plus, **136**(2), 156(2021); https://doi.org/10.1140/epjp/s13360-021-01125-4
[57] Shaaban, K. S., Al-Baradi, A. M., & Ali, A. M., Silicon, **14**(4), 10375-10382(2022); https://doi.org/10.1007/s12633-022-01783-8
[58] Al-Baradi, A. M., Wahab, E. A. A., & Shaaban, K. S., Silicon, **14**(3), 5277-5287(2022); https://doi.org/10.1007/s12633-021-01286-y